Two long-axis dimensions of hippocampal-cortical integration support memory function across the adult lifespan

Kristin Nordin[*1,2,3], Robin Pedersen[3,4,5], Farshad Falahati[1,2], Jarkko Johansson[4,6], Filip Grill[7], Micael Andersson[4,5], Saana M. Korkki[1,2], Lars Bäckman[1,2], Andrew Zalesky[8,9], Anna Rieckmann[4,5,6,10], Lars Nyberg[4,5], Alireza Salami[1,2,3,4,5]

[*]Corresponding author

[1]Department of Neurobiology, Care Sciences, and Society, Karolinska Institutet, Solna, Sweden

[2]Aging Research Center, Karolinska Institutet and Stockholm University, Solna, Sweden

[3]Wallenberg Centre for Molecular Medicine, Umeå University, Umeå, Sweden

[4]Umeå Center for Functional Brain Imaging, Umeå University, Umeå, Sweden

[5]Department of Integrative Medical Biology, Umeå University, Umeå, Sweden

[6]Department of Radiation Sciences, Umeå University, Umeå, Sweden

[7]Centre for Cognitive Neuroimaging, Donders Institute for Brain, Cognition and Behaviour, Radboud University, Nijmegen, The Netherlands

[8]Department of Biomedical Engineering, the University of Melbourne, Melbourne, VIC, Australia

[9]Department of Psychiatry, the University of Melbourne, Melbourne, VIC, Australia

[10]Department of Psychology, University of the Bundeswehr Munich, Germany

Corresponding author: Kristin Nordin

Karolinska Institutet

Aging Research Center

Tomtebodavägen 18A

171 65 Solna, Sweden

E-mail: kristin.nordin@ki.se

Abstract

The hippocampus is a complex structure critically involved in numerous behavior-regulating systems. In young adults, multiple overlapping spatial modes along its longitudinal and transverse axes describe the organization of its functional integration with neocortex, extending the traditional framework emphasizing functional differences between sharply segregated hippocampal subregions. Yet, it remains unknown whether these modes (i.e., gradients) persist across the adult human lifespan, and relate to memory and molecular markers associated with brain function and cognition. In two independent samples, we demonstrate that the principal anteroposterior and second-order, mid-to-anterior/posterior hippocampal modes of neocortical functional connectivity, representing distinct dimensions of macroscale cortical organization, manifest across the adult lifespan. Specifically, individual differences in topography of the second-order gradient predicted episodic memory and mirrored dopamine D1 receptor distribution, capturing shared functional and molecular organization. Older age was associated with less distinct transitions along gradients (i.e., increased functional homogeneity). Importantly, a youth-like gradient profile predicted preserved episodic memory – emphasizing age-related gradient dedifferentiation as a marker of cognitive decline. Our results underscore a critical role of mapping multidimensional hippocampal organization in understanding the neural circuits that support memory across the adult lifespan.

Key words: Adult lifespan, Aging, Anteroposterior axis, Brain maintenance, Brain organization, Connectopic mapping, Dopamine, Episodic memory, Functional connectivity, Hippocampus

The hippocampus plays a critical role in human behavior beyond its well-established involvement in memory and spatial navigation[1–3]. Contemporary views hold that its broad involvement in cognition emerges through the combination of its intrinsic circuitry and its widespread neocortical connections – placing it at the interface of multiple behavioral systems[2,4]. Characterizing organizational principles of hippocampal integration with the larger neocortical landscape is therefore key to our understanding of its contribution to cognition and to the many diseases associated with its dysfunction[5–8].

Animal models[9,10], together with histological and functional descriptions in humans[11–13], emphasize the hippocampus transverse (mediolateral) and longitudinal (anteroposterior) axes in determining its functional organization, contribution to behavior[14,15], and vulnerability to neurological disease[16,17]. In humans, functional analogues of the hippocampus canonical internal circuitry and its anatomical connections with neocortical areas have successfully been provided by resting-state functional magnetic resonance imaging (fMRI)[12,18], at a coarse scale confirming the anteroposterior differentiation in connectivity observed in the animal literature[9,19,20]. Despite the consistency by which this anteroposterior organizational dimension emerges[21], significant questions however remain regarding its spatial distribution across cortex and its contribution to behavior across the adult human lifespan.

Lack of consensus is especially evident in terms of the hippocampus functional connectivity with the default-mode network (DMN), encompassing core areas of the brain's system for memory-guided behavior[4,22]. Several studies primarily attribute integration with the DMN to the posterior hippocampus[4,12,23,24], consistent with its anatomical connections to midline posterior parietal areas[19]. Other sources emphasize the anterior hippocampus as driving connectivity with the DMN[25–27], on the basis of its anatomical connections with ventromedial prefrontal areas[19]. These inconsistencies ultimately limit our understanding of hippocampal functional specialization, and the impact on cognition of the heterogeneous vulnerability to

aging and disease observed along the hippocampus longitudinal axis[17,28]. We propose that inconsistencies in part stem from overlooking multiple overlapping and complementary functional modes, not discernable through traditional parcellation-based approaches, which assume homogeneous function within distinct, pre-defined, portions of the hippocampus.

Accumulating evidence in young adults indicate that hippocampal neocortical connectivity is indeed fundamentally multidimensional – organized in several overlapping, but distinct, spatial modes[21,29–32]. Whereas such gradient-based observations describe a principal anteroposterior mode of neocortical connectivity, they also identify orthogonal modes of long-axis and transverse variation in connectivity[29–31]. Importantly, these hippocampal gradients appear to reflect well-known gradients of macroscale brain function[31], which express functional differentiation across distinct cortical hierarchies[33,34]. The principal anteroposterior gradient has been linked to functional differentiation along a task-negative/task-positive cortical dimension[35], separating neural communities involved in the formation of representations from sensory input (e.g., visual, somatosensory, and DMN areas) and those involved in the modulation of these representations (e.g., frontoparietal areas of attention and control)[31,34]. In parallel, a secondary, non-linear, long-axis gradient is suggested to correspond to the principal unimodal-transmodal gradient of cortical function (oppositely anchored in associative DMN areas and in unimodal sensory and motor cortices[33,34])[31]. However, the biological underpinnings of this secondary gradient are still unknown, in contrast to the principal gradient, demonstrated also in microstructure[23], gray matter covariance[13,36], and gene expression[37].

Differences in the topography (i.e., the spatial layout) of the principal, anteroposterior, hippocampal gradient may predict episodic memory[30], but current findings are restricted to younger age – and to mainly the same sample (i.e., the Human Connectome Project[38])[29–31]. Moreover, it remains unknown in which capacity the secondary long-axis gradient contributes to behavior. Yet, a comprehensive model of the spatial properties of

hippocampal functional organization should consider that hippocampal functional alterations occur across the adult lifespan, and manifest across the hippocampus in a heterogeneous manner. Specifically, aging has been linked to differential functional isolation of anterior and posterior hippocampal regions from prefrontal areas and large-scale brain networks including the DMN[39,40]. Such neocortical disconnection of hippocampal subregions has been linked to dysfunction during memory encoding and retrieval[40–42], and in turn, to episodic memory decline[42]. Findings which link hippocampal isolation to increased functional homogeneity within the region, suggest that its disconnection from neocortex is driven by the spatial patterns in which Alzheimer's disease (AD) pathology accumulates in cognitively healthy older adults[43,44]. Importantly, loss of functional segregation between task-negative and task-positive poles is a functional hallmark of both healthy aging[45] and AD[46] – introducing overall ambiguity as to whether hippocampal gradients established in young adults persist into older age.

Dopamine (DA) is one of the most important modulators of hippocampus-dependent function[47,48], and influences the brain's functional architecture through enhancing specificity of neuronal signaling[49]. Consistently, there is a DA-dependent aspect of maintained functional network segregation in aging which supports cognition[50]. Animal models suggest heterogeneous patterns of DA innervation[51,52] and postsynaptic DA receptors[53], across both transverse and longitudinal hippocampal axes, likely allowing for separation between DA modulation of distinct hippocampus-dependent behaviors[47]. Moreover, the human hippocampus has been linked to distinct DA circuits on the basis of long-axis variation in functional connectivity with midbrain and striatal regions[54,55]. Taken together with recent findings revealing a unimodal-transmodal organization of the most abundantly expressed DA receptor subtype, D1 (D1DR), across cortex[56], we tested the hypothesis that the organization of hippocampal-neocortical connectivity partly reflects the underlying distribution of

hippocampal DA receptors, predicting predominant spatial correspondence for any hippocampal gradient conveying a unimodal-transmodal pattern across cortex.

Here, we characterize the multidimensional functional organization of the hippocampus in two independent adult-lifespan samples, and map individual differences in fine-scale topographic properties of connectivity gradients onto behavioral and molecular phenotypes. We report three hippocampal gradients displaying distinct correspondence to a) canonical gradients of cortical function, b) the organization of hippocampal DA receptors, and c) individual differences in memory function. Multivariate, data-driven, classification on gradient topography identified older adults exhibiting a youth-like gradient profile and superior memory function as distinct from age-matched older counterparts, emphasizing a behavioral significance of preserved functional hippocampal topography in older age.

Results

Multiple dimensions of hippocampal-neocortical integration across the adult lifespan

Connectopic mapping[57] was applied to resting-state fMRI data (n=180, 90 men/90 women; 20-79 years; mean age = 49.8±17.4) from the DyNAMiC study[58]. For replication, we used an independent sample of 224 adults (122 men/102 women; 29-85 years mean age = 65.0±13.0) from the Betula project[59]. Connectopic mapping was used to extract the dominant modes of functional cortical connectivity within the hippocampus based on non-linear manifold learning (Laplacian eigenmaps) applied to a similarity matrix derived from connectivity fingerprints computed between each hippocampal voxel and each voxel within neocortex. This identified a set of orthogonal connectopic maps (i.e., eigenvectors) describing overlapping connectivity topographies (i.e., gradients) within the hippocampus. Gradients were computed at subject level, and at group level across the sample, separately for the left and right hippocampus. We analyzed the first three gradients, together explaining 63% and 71% of the variance in left and

right-hemispheres, respectively. This number corresponded to a clear elbow in the scree plot (Supplementary Figure 1).

The principal gradient (G1), explaining 44% and 53% of the variance in left and right hemispheres, was organized along the hippocampus longitudinal axis, conveying gradual anterior-to-posterior variation in cortical connectivity (Figure 1A). This pattern of connectivity change is illustrated by dividing subject-level G1 connectopic maps into 23 long-axis bins of ~2mm and plotting the average gradient values as a function of their distance from the most anterior hippocampal voxel[30] (Figure 1B). The second-order gradient (G2), explaining 11% of the variance in both hemispheres, expressed a secondary long-axis gradient organized from the middle hippocampus towards anterior and posterior ends (Figure 1A-B). Finally, the third-order gradient (G3: explaining 8% and 7% of the variance), reflected variation along the hippocampus transverse axis, such that inferior-lateral parts of the hippocampus were separated from medial-superior parts (Figure 1A). This pattern was most pronounced in the anterior hippocampus. Inspecting G3 across sample-specific segmentations of cornu ammonis (CA1-3), dentate gyrus (DG/CA4), and subiculum subfields suggested that while CA1-3 expressed the full extent of the gradient, and DG/CA4 variation around its center, the subiculum expressed only the most inferior section of the gradient (Supplementary Figure 2).

The three gradients reflected gradients identified in young adults[29–31], and were highly reproducible in the independent replication data set (Supplementary Figure 3). Correspondence between samples was determined by spatial correlations (left hemisphere: G1: $r = 0.990$, $p < 0.001$; G2: $r = 0.946$, $p < 0.001$; G3: $r = 0.918$, $p < 0.001$; right hemisphere: G1: $r = 0.996$, $p < 0.001$; G2: $r = 0.969$, $p < 0.001$; G3: $r = 0.897$, $p < 0.001$). Furthermore, the reliability of connectopic mapping to produce functional connectivity gradients was determined across varying degrees of spatial smoothing, and contrasted against connectopic maps derived from random data[60]. Results confirmed high stability of resting-state gradients and their efficacy

in capturing inter-individual differences, whereas random data failed to produce meaningful gradients (Supplementary Figure 4).

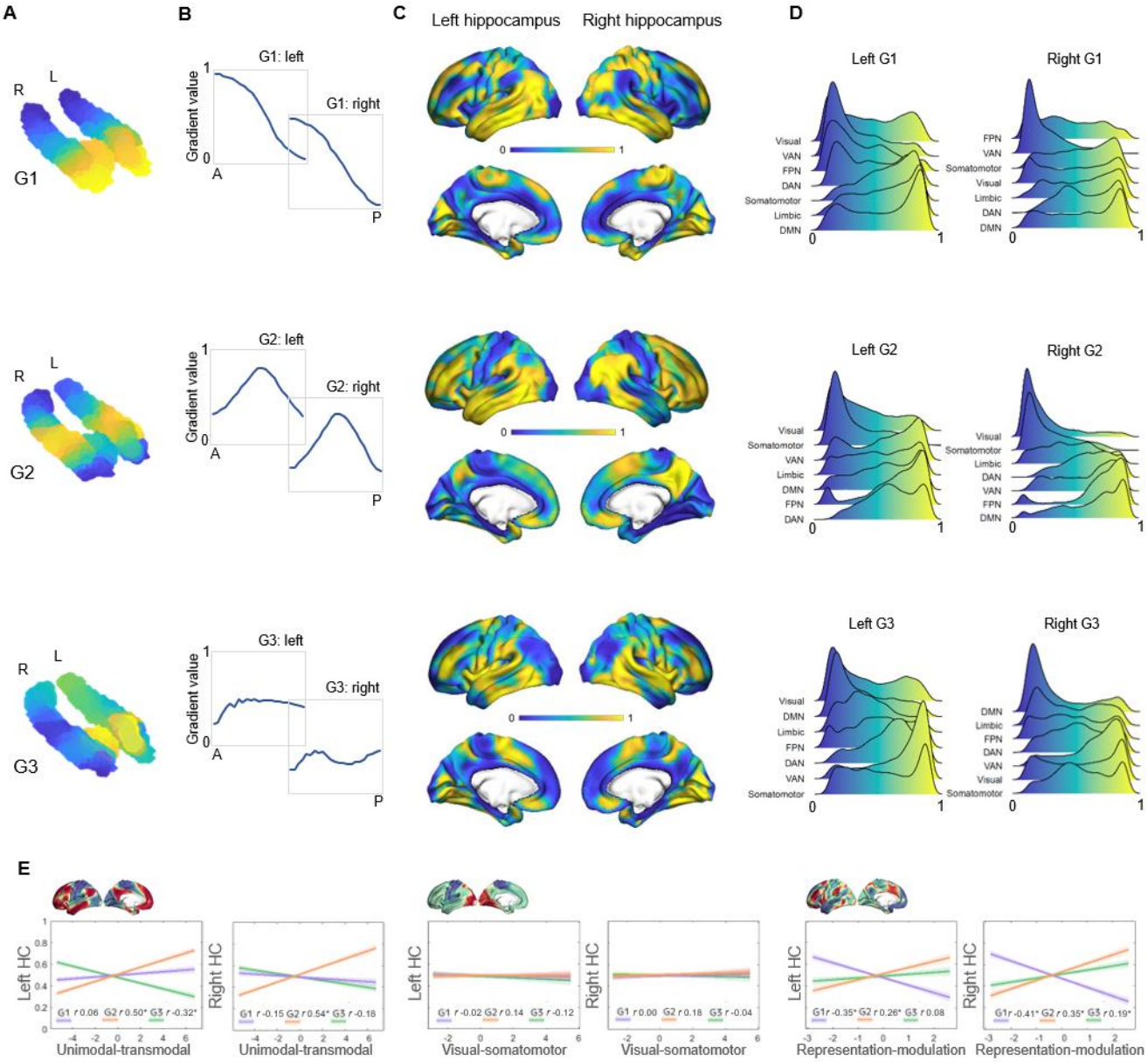

Figure 1. Topographic gradients of hippocampal cortical connectivity. A) The first three hippocampal connectopic maps (G1-G3), explaining 67% of the variance across left and right hemispheres. Similar colors convey similar patterns of cortical connectivity. Values range between 0 (blue) and 1 (yellow). B) Plots convey change in connectivity along the anteroposterior hippocampal axis. Mean values from 23 hippocampal bins (each ~2mm) are plotted against their distance (in mm) from the most anterior hippocampal voxel. Values were estimated based on subject-level gradients and averaged across participants. G1 conveys gradual change in connectivity along an anteroposterior gradient. G2 conveys gradual change in connectivity along a second-order long-axis gradient, separating the middle hippocampus from anterior and posterior ends. G3 conveys close to no change in connectivity along the longitudinal axis, with connectivity change instead organized in a primarily medial-lateral gradient. C) Cortical projections for G1, G2, and G3. Values range between 0 (blue) and 1 (yellow). D) The order of cortical networks in gradient space. Density plots visualize the distribution of gradient values for seven cortical networks (Yeo et al., 2011). E) Correlations between cortical patterns of hippocampal gradients and the three primary gradients of cortical functional organization, which are exemplified at the top of each graph (Margulies et al., 2016).

Hippocampal gradients reflect distinct dimensions of macroscale cortical organization

The projection of G1 onto cortex conveyed a pattern linking medial orbitofrontal, temporolimbic, and medial parietal regions at the anterior end of the gradient with occipital and frontoparietal regions at the posterior end (Figure 1C). For further characterization, we computed G1 gradient values within seven cortical networks[61], and examined their position in gradient space. This placed the DMN, limbic, and somatomotor networks at anterior-to-middle parts of the gradient, whereas visual, ventral attention, and frontoparietal networks toward the posterior end of the gradient (Figure 1D). In contrast, G2 exhibited a unimodal-transmodal pattern across cortex, linking the middle hippocampus to frontal and posterior parietal regions, and anterior and posterior hippocampal ends to somatomotor and occipital regions (Figure 1C). Consistently, the DMN and frontoparietal network mapped onto G2 at one end, and visual and somatomotor networks at the other (Figure 1D). Across cortex, G3 primarily separated temporal and insular areas from medial parietal and medial frontal areas (Figure 1C). Aligning with cortical connectivity previously reported for hippocampal subfields[29,62], areas of the DMN most strongly mapped onto the most inferior end of G3, consistent with the connectivity profile of the subiculum, whereas ventral attention and somatomotor networks had a stronger medial position along G3, aligning with reported connectivity of CA1-3 (Figure 1D).

Next, we linked the cortical patterns of gradients to the established macroscale layout of cortical function[34] using Spearman's rank correlation analyses. G1 showed significant correspondence with the cortical representation-modulation gradient[34], differentiating the task-negative DMN and somatomotor networks from task-positive areas of attention and control (left G1: Spearman's r = -0.353, $p_{spin} < 0.001$; right G1: Spearman's r = -0.406, $p_{spin} < 0.001$; Figure 1E). G1's correlation with this cortical gradient was greater than its correlations to other cortical gradients ($6.3 < Z < 9.6$, $ps < 0.001$), as well as significantly stronger than correlations observed for G2 and G3 ($1.6 < Z < 6.5$, $ps < 0.05$). In contrast, G2 corresponded to the principal

unimodal-transmodal gradient of cortical function (left G2: Spearman's $r = 0.502$, $p_{spin} < 0.001$; right G2: Spearman's $r = 0.536$, $p_{spin} < 0.001$; Figure 1E), to a greater extent than G1 and G3 ($4.9 < Z < 10.9$, $ps < 0.001$) and in comparison to other cortical gradients ($5.2 < Z < 9.4$, $ps < 0.001$). Finally, the cortical pattern of G3 showed overall weaker correspondence with the canonical cortical gradients. G3's correlations with the unimodal-transmodal gradient (left G3: Spearman's $r = -0.32$, $p_{spin} = 0.011$), and the representation-modulation gradient (right G3: Spearman's $r = 0.191$, $p_{spin} = 0.009$), were significantly weaker compared their counterparts of G2 ($Z_{(998)} = 4.9$, $p < 0.001$) and G1 ($Z_{(998)} = 5.3$, $p < 0.001$). These multiple lines of evidence contribute to a model of hippocampal functional organization across the adult human lifespan in which G1 and G2 constitute local representations of distinct macroscale cortical motifs.

Distinct patterns of behavioral transitions along G1 and G2

Given the correspondence of G1 and G2 to distinct gradients of cortical function, we characterized their relevance for hippocampal functional specialization by mapping transitions in behavioral domains onto G1 and G2 using meta-analytical decoding in Neurosynth[63]. Correlations were assessed between meta-analytical maps of behavioral terms and twenty-percentile bins of each gradient's cortical projection (Figure 2). First, a selection of terms commonly linked to anteroposterior hippocampal functional specialization[13,14] were assessed across G1 and ranked based on their location along the gradient (Figure 2A). The strongest anterior loadings on G1 belonged to terms including *words*, *social*, and *dementia*, whereas terms of *navigation*, *episodic memory*, *encoding*, and *recollection* showed preferential posterior loadings. In contrast, behavioral transitions along G2 were expected to reflect its unimodal-transmodal organization (Figure 1B). To this end, terms were selected and ordered based on a previous report demonstrating unimodal-transmodal behavioral transitions across cortex[34]. G2 expressed a clear separation between *sensorimotor* and *visual* terms at one end from *social*,

self-referential, and *default* terms at the other (Figure 2B), confirming its unimodal-transmodal organization.

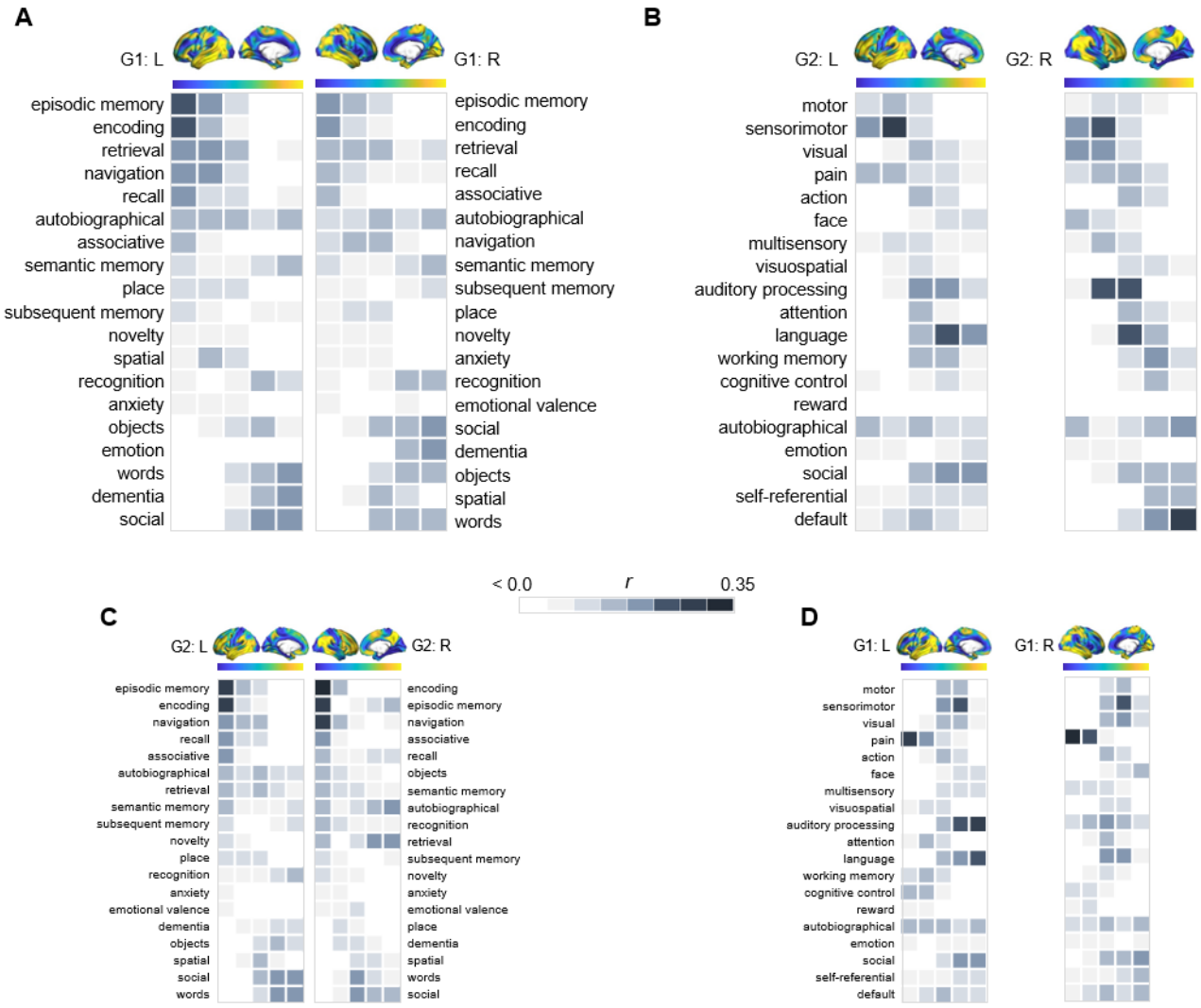

Figure 2. Behavioral profiling of G1 and G2 across cortex. For each gradient, columns represent twenty-percentile bins of the gradient's cortical projection. Color shadings represent the strength of correlations between gradient bins and meta-analytical maps in Neurosynth. A) Terms commonly linked to anteroposterior hippocampal functional specialization were assessed across G1 and ranked based on their location along the gradient. B) For G2, terms were selected and ordered as to reflect a unimodal-transmodal cortical axis[34]. C) The correspondence between G2 and behavioral terms commonly linked to anteroposterior hippocampal functional specialization. D) The correspondence between G1 and behavioral terms expressing a unimodal-transmodal axis.

Topography of G2 reflects distribution of hippocampal dopamine D1 receptors

Our next aim was to investigate to which extent the distribution of hippocampal DA D1 receptors (D1DRs), measured by [^{11}C]SCH23390 PET in the DyNAMiC[58] sample, may serve as a molecular correlate of the hippocampus' functional organization. First, to estimate individual differences in gradients' spatial layout, trend surface modelling (TSM) was applied to each subject-level connectopic map[30,57,64]. This spatial-statistics approach parameterizes gradients at subject level, yielding a set of model parameters describing the topographic characteristics of each gradient in x, y, z directions (see Methods, and Supplementary Figure 5 for model selection). Unlike voxel-wise statistical inference on gradients, which overlooks the high interdependence between voxels' gradient values and demands rigorous correction for multiple comparisons, TSM allows for statistical inference across a region's internal heterogeneity using a concise set of independent parameters[64]. Moreover, by adjusting the number of polynomial terms, TSM facilitates examination of spatial trends across gradients at coarser-to-finer levels[64].

Individual maps of D1DR binding potential (BP) were also submitted to TSM, yielding a set of spatial model parameters describing the topographic characteristics of hippocampal D1DR distribution for each participant. D1DR parameters were subsequently used as predictors of gradient parameters in one multivariate GLM per gradient (in total 6 GLMs, controlled for age, sex, and mean FD). Results are reported with p-values at an uncorrected statistical threshold and p-values after adjustment for multiple comparisons using the Benjamini-Hochberg method to control the false discovery rate (FDR). Individual differences in D1DR topography significantly explained topography of right-hemisphere G2 ($F = 1.207$, $p = 0.041$, $p_{FDR} = 0.073$; partial $\eta 2 = 0.118$), but not of G1 nor G3 (F 0.953-1.108, p 0.222-0.596) (Figure 3). This association was robust across multiple TSM model orders (Supplementary Figure 6). Complimentary analyses were then conducted to further evaluate G2 as a

dopaminergic hippocampal mode by utilizing additional DA markers at group-level. First, a map of D1DR distribution was formed by averaging the [^{11}C]SCH23390 BP images across DyNAMiC participants (n=176), and a map of D2DR distribution was formed by averaging [^{11}C]raclopride BP images in a subsample of DyNAMiC participants (n = 20). Previously published maps of DAT[65] and FDOPA (https://www.nitrc.org/projects/spmtemplates) were also analyzed. Correlations across group-level TSM parameters[66], revealed significant positive associations between G2 and D1, DAT, and FDOPA (D1: r = 0.501, p < 0.01, p_{FDR} = 0.021; DAT: r = 0.378, p < 0.01, p_{FDR} = 0.021; FDOPA: r = 0.584, p < 0.01, p_{FDR} = 0.021; Figure 3C), although not D2 (D2: r = 0.131, p = 0.440, p_{FDR} = 0.528), whereas correlations were not significant for G1 or G3, indicating that G2 best captures shared principles of functional and molecular organization.

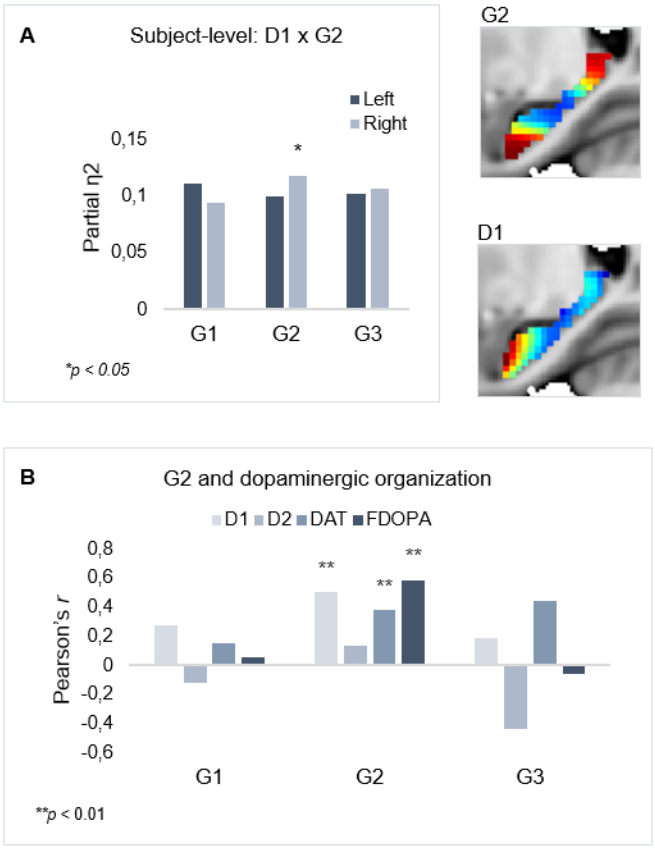

Figure 3. Shared functional and molecular organization within the hippocampus. A) Multivariate effects of hippocampal D1DR TSM parameters as predictors of G2 TSM parameters. Images show average organization of G2 and D1DR in the right hemisphere. Note that the arbitrary color scale of G2 has been flipped. B) Correlations between group-level TSM parameters of functional gradients and DA markers.

Dedifferentiated gradient topography in older age

Effects of age on gradient topography were assessed using multivariate GLMs including age as the predictor and gradient TSM parameters as dependent variables (controlling for sex and mean frame-wise displacement; FD). One model was fitted per gradient and hemisphere, each model including all TSM parameters belonging to a gradient (in total, 6 GLMs). There was a significant effect of age on topographic characteristics of all three gradients. G1 displayed the greatest effect of age (left: $F_{(9,150)} = 5.853$, $p < 0.001$, $p_{FDR} = 0.003$, partial $\eta^2 = 0.260$; right: $F_{(9,150)} = 6.971$, $p < 0.001$, $p_{FDR} = 0.003$, partial $\eta^2 = 0.298$), followed by G2 (left: $F_{(12,147)} = 2.583$, $p = 0.004$, $p_{FDR} = 0.01$, partial $\eta^2 = 0.174$; right: $F_{(12,145)} = 2.635$, $p = 0.003$, $p_{FDR} = 0.008$, partial $\eta^2 = 0.179$), and G3 (left: $F_{(12,147)} = 1.973$, $p = 0.030$, $p_{FDR} = 0.056$, partial $\eta^2 = 0.139$; right: $F_{(12,145)} = 2.082$, $p = 0.021$, $p_{FDR} = 0.042$, partial $\eta^2 = 0.147$). To visualize effects, subject-level G1 and G2 values were plotted along the anteroposterior axis, averaged within young (20-39 years), middle-aged (40-59 years) and older (60-79 years) adults. Connectivity across G1 and G2 displayed less distinct differentiation at older age, depicted by the flatter curves in the older group (Figure 4A). The difference in gradient values between each consecutive pair of gradient bins was computed, and the locations of significant univariate contributions to the effect of age on these values were visualized along gradients (Figure 4B-C). For G1, this primarily localized effects to a middle hippocampal region extending posteriorly from just after the uncal apex (MNI y=21).

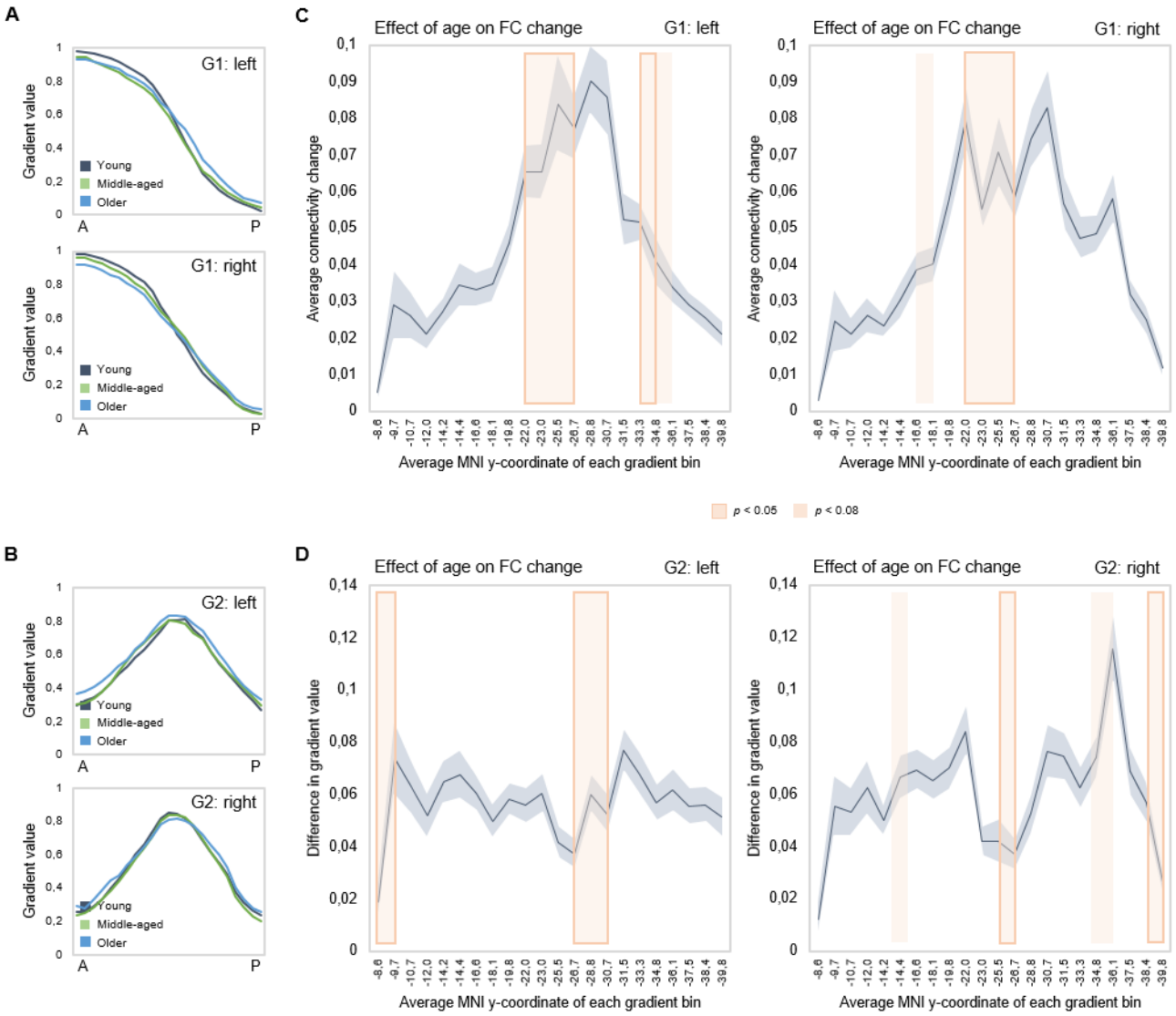

Figure 4. Effects of age on hippocampal gradients. A-B) Less specificity in connectivity change across G1 and G2 in older age. Average values of subject-level gradient bins are plotted as a function of their distance from the most anterior hippocampal voxel. Separate lines mark young (20-39 years; gray), middle-aged (40-59 years, green), and older (60-79 years; blue) age groups. The flatter curves in the older group indicate less distinct change in connectivity patterns across gradients in older age. C) Localization of age effects along G1. Shaded fields indicate the position of significant age effects along G1. D) Localization of age effects along G2. Shaded fields indicate the position of significant age effects along G2.

Topography of hippocampal gradients predicts episodic memory performance

Next, we tested associations between topography of the three gradients and episodic memory. Using hierarchical multiple regression models in which age, sex, and mean FD were controlled for in a first step (M1), we entered TSM parameters of the three gradients as predictors of episodic memory in a step-wise manner. Models were assessed separately for left and right hemispheres, across the full sample and within age groups, yielding eight hierarchical models in total. Results are reported with p-values at an uncorrected statistical threshold and p-values after FDR adjustment. Memory performance was, across the sample, predicted by G2 in the left hippocampus (Adj. $R^2 = 0.308$, $\Delta R^2 = 0.096$, F= 1.842, $p = 0.047$, $p_{FDR} = 0.082$) over and above covariates and topography of G1, which did not predict performance (Adj. $R^2 = 0.260$, $\Delta R^2 = 0.029$, F= 0.695, $p = 0.713$, $p_{FDR} = 0.771$), and neither did G3 (Adj. $R^2 = 0.276$, $\Delta R^2 = 0.027$, F= 0.502, $p = 0.910$, $p_{FDR} = 0.920$), Figure 5A. Observing that the association between G2 and memory did not remain significant after FDR adjustment, we performed the same analysis in our replication dataset, which also included episodic memory testing. Consistent with the observation in our main dataset, G2 significantly predicted memory performance (Adj. $R^2 = 0.368$, $\Delta R^2 = 0.081$, F= 1.992, $p = 0.028$) over and above covariates and topography of G1. Here, the analysis also showed that G1 topography predicted performance across the sample (Adj. $R^2 = 0.325$, $\Delta R^2 = 0.112$, F= 3.431, $p < 0.001$).

In our main dataset, memory performance was within young adults, predicted by left-hemisphere G1 (Adj. $R^2 = 0.182$, $\Delta R^2 = 0.357$, F= 2.672, $p = 0.015$, $p_{FDR} = 0.030$), whereas neither G2 (Adj. $R^2 = 0.204$, $\Delta R^2 = 0.191$, F= 1.098, $p = 0.396$, $p_{FDR} = 0.492$) nor G3 (Adj. $R^2 = 0.384$, $\Delta R^2 = 0.236$, F= 1.755, $p = 0.132$, $p_{FDR} = 0.189$) improved the prediction (Figure 5B). No gradient predicted memory within middle-aged or older age groups (F 0.432-1.865, p 0.928-0.113; Supplementary Table 1).

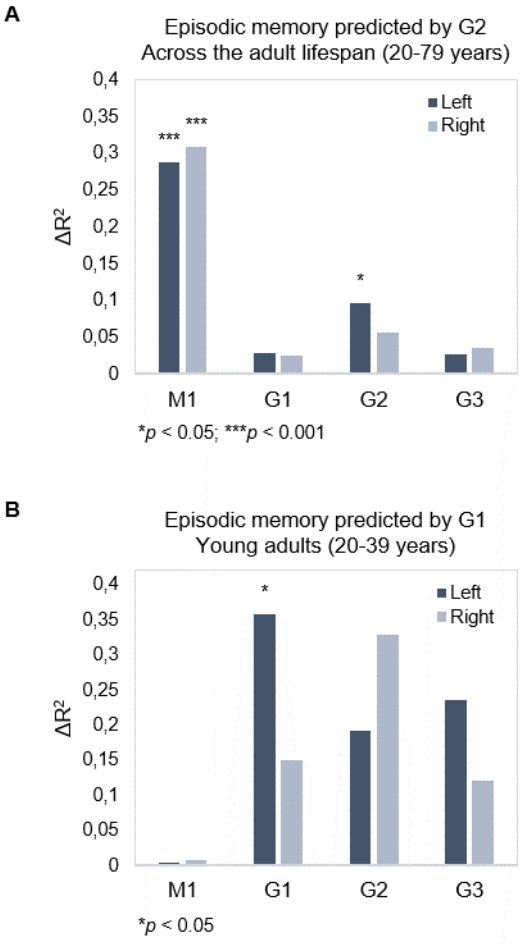

Figure 5. Gradient topography and episodic memory. A) Individual differences in topographic characteristics of left-hemisphere G2 significantly predicted episodic memory performance across the sample, over and above the first- and second-step models (M1: age, sex, in-scanner motion; G1 parameters). B) Topographic characteristics of G1 in the left hemisphere significantly predicted episodic memory performance in young adults, over and above M1 (age, sex, and in-scanner motion).

Youth-like gradient topography supports memory in older age

To investigate the functional role of G1 in old age, the principal and most age-sensitive gradient, we tested whether memory in older adults would be facilitated by youth-like gradient topography using two independent datasets. In DyNAMiC, we applied data-driven latent class analysis (LCA) to TSM parameters (residualized to account for age, sex, and mean FD) of left-hemisphere G1, which predicted episodic memory performance in younger adults. LCA yielded a two-class solution identifying two subgroups (n=19 vs. n=30) of older adults (60-79 years), which by definition differed in left-hemisphere G1 characteristics ($F_{(9,37)} = 13.778$, $p < 0.001$, $p_{FDR} = 0.003$, partial $\eta^2 = 0.770$). A difference was also evident in the right hemisphere ($F_{(9,37)} = 3.790$, $p = 0.002$, $p_{FDR} = 0.005$, partial $\eta^2 = 0.480$).

Individuals in the smaller subgroup were determined as exhibiting an aged gradient profile, whereas older adults in the larger subgroup as exhibiting a youth-like gradient profile. The classification based on G1 parameters extended across all three gradients in both hemispheres (Figure 6A), such that the smaller subgroup displayed marked differences from younger adults across all gradients (left G1: $F_{(9,63)} = 15.549$, $p < 0.001$, $p_{FDR} = 0.003$, partial $\eta^2 = 0.690$; right G1: $F_{(9,63)} = 5.322$, $p < 0.001$, $p_{FDR} = 0.003$, partial $\eta^2 = 0.432$; left G2: $F_{(12,60)} = 3.991$, $p < 0.001$, $p_{FDR} = 0.003$, partial $\eta^2 = 0.444$; right G2: $F_{(12,60)} = 2.192$, $p = 0.023$, $p_{FDR} = 0.045$, partial $\eta^2 = 0.305$; left G3: $F_{(12,60)} = 2.832$, $p = 0.004$, $p_{FDR} = 0.01$, partial $\eta^2 = 0.362$; right G3: $F_{(12,60)} = 1.844$, $p = 0.061$, $p_{FDR} = 0.098$, partial $\eta^2 = 0.269$), while the larger subgroup differed less from young adults in terms of G1 (left G1: $F_{(9,74)} = 4.416$, $p < 0.001$, $p_{FDR} = 0.003$, partial $\eta^2 = 0.349$; right G1: $F_{(9,74)} = 3.086$, $p = 0.003$, $p_{FDR} = 0.008$, partial $\eta^2 = 0.273$), and displayed second- and third-order gradients comparable to those in younger age (left G2: $F_{(12,71)} = 1.616$, $p = 0.107$, $p_{FDR} = 0.167$, partial $\eta^2 = 0.215$; right G2: $F_{(12,71)} = 1.442$, $p = 0.168$, $p_{FDR} = 0.235$, partial $\eta^2 = 0.196$; left G3: $F_{(12,71)} = 1.122$, $p = 0.357$, $p_{FDR} = 0.457$, partial $\eta^2 = 0.159$;

right G3: $F_{(12,71)} = 1.596$, $p = 0.112$, $p_{FDR} = 0.172$, partial $\eta^2 = 0.212$). See Supplementary Figure 7 for classification based on right-hemisphere G1.

Plotting connectivity change along G1 and G2 in the aged and youth-like subgroups revealed that the diminished topographic specificity observed across gradients in older individuals (Figure 4A) was driven by older adults with an aged gradient profile (Figure 6B). Both older subgroups displayed altered gradient organization across cortex (Figure 6C-D). The distribution of cortical networks in G1 space indicated a unimodal-transmodal organization in youth-like older adults, not evident in the aged older group (Figure 6D). The two groups did not differ in terms of age (aged: 70.8±6.0; youth-like: 68.4±4.7; $t = 1.548$, $p = 0.128$, $p_{FDR} = 0.189$), sex (aged: 9 men/10 women; youth-like: 16 men/14 women; $X^2 = 0.166$, $p = 0.684$, $p_{FDR} = 0.746$), nor hippocampal gray matter (left hemisphere: aged: 4271.2 ml ±480.9; youth-like: 4246.8 ml ±269.1; $t = 0.223$, $p = 0.824$, $p_{FDR} = 0.850$; right hemisphere: aged: 3866.2 ml ±446.3; youth-like: 3979.9 ml ±398.1; $t = 0.929$, $p = 0.357$, $p_{FDR} = 0.457$). Subgroups showed comparable levels of average hippocampal D1DR availability (left: youth-like 0.257±0.06; aged 0.242±0.06; $t = 0.796$, $p = 0.430$, $p_{FDR} = 0.525$; right: youth-like 0.242±0.06; aged 0.251±0.06 $t = 0.296$, $p = 0.768$, $p_{FDR} = 0.817$), but displayed a pattern of differences in D1DR TSM parameters in comparison to young adults supporting youth-like and aged profiles (youth-like subgroup vs. young: left: $F_{(9,74)} = 1.645$, $p = 0.118$, $p_{FDR} = 0.176$, partial $\eta^2 = 0.167$; aged subgroup vs. young: left: $F_{(9,62)} = 3.478$, $p = 0.002$, $p_{FDR} = 0.005$, partial $\eta^2 = 0.335$; Figure 6E).

In line with our hypothesis, we observed superior memory in older adults exhibiting a youth-like gradient profile (Figure 6E): at trend-level for the composite episodic measure (aged: 43.2±3.7; youth-like: 46.5±6.6; $t = 1.958$, $p = 0.056$, $p_{FDR} = 0.092$), driven by a significant group difference on its word recall sub test (aged: 40.9±4.5; youth-like: 43.4±6.8; $t = 2.600$, $p = 0.012$, $p_{FDR} = 0.025$). Word recall performance was furthermore predicted by left-hemisphere G1 parameters (over and above age, sex, and mean FD) in the youth-like older

adults (Adj. $R^2 = 0.464$, $\Delta R^2 = 0.543$, $F = 3.043$, $p = 0.028$, $p_{FDR} = 0.054$), while no association was observed in the aged older subgroup (Adj. $R^2 = 0.063$, $\Delta R^2 = 0.533$, $F = 1.004$, $p = 0.518$, $p_{FDR} = 0.599$). Crucially, the ability of left G1 topography to inform classification of older adults into mnemonically distinct subgroups was replicated in the Betula sample (Supplementary Information; Figure 7C).

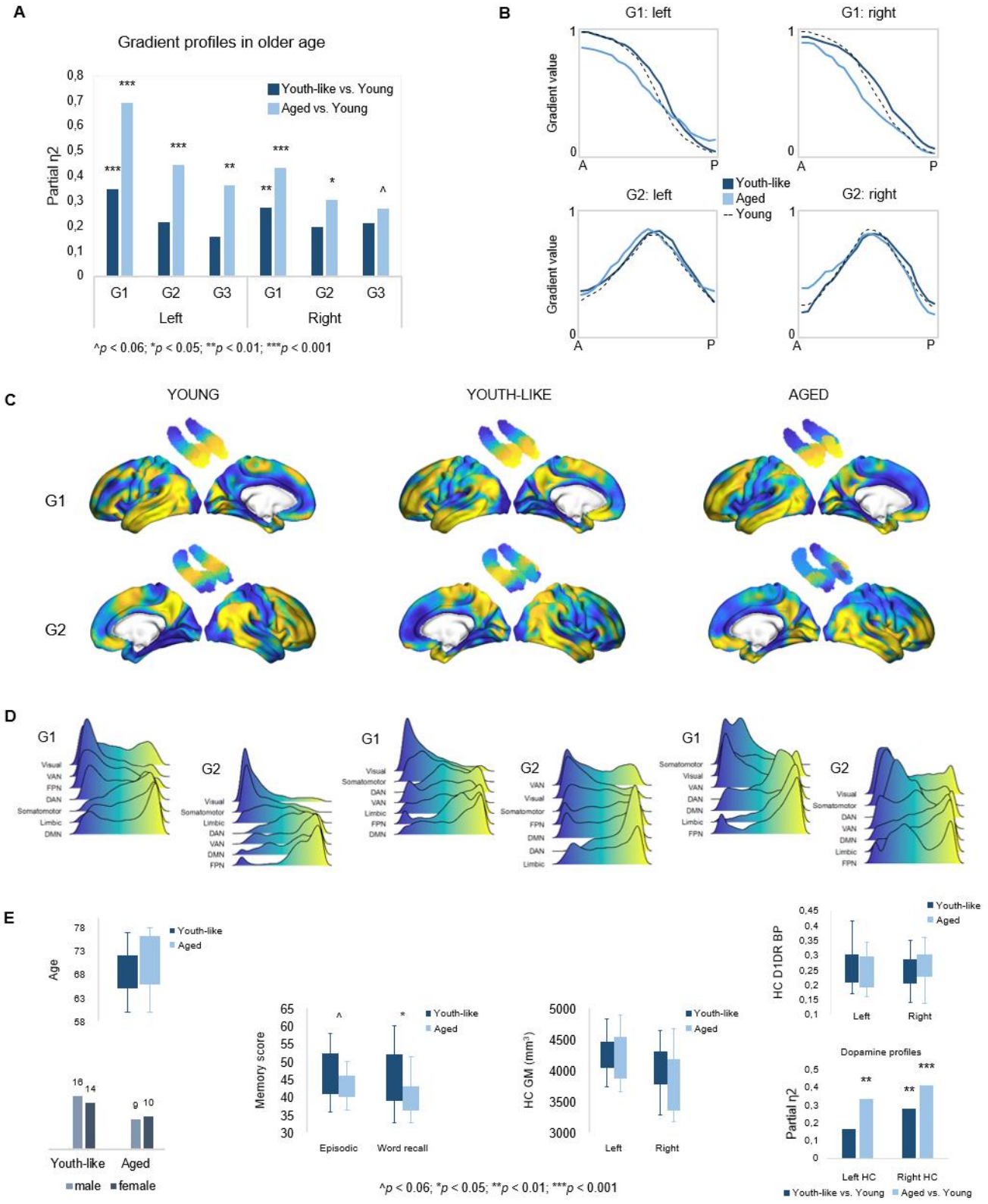

Figure 6. Gradient profiles in older age. A) Two older subgroups were identified based on left-hemisphere G1. The first group (n=19) displayed gradient characteristics significantly different from those in young adults, whereas the second group (n=30) displayed gradient characteristics more similar to those in young adults. Bars represent comparisons of gradient TSM parameters between older subgroups and younger adults. B) Average gradient values across participants within subgroups, plotted against the distance (in mm) from the most anterior hippocampal voxel. The flatter curves in older adults with an aged gradient profile suggest less distinct change in connectivity across gradients. C) Group-level G1 and G2 for young, youth-like, and aged groups. D) Position of cortical networks in gradient space. E) Older subgroups were comparable in terms of age, sex, hippocampal gray matter volume, and average levels of hippocampal D1DR availability, while older adults with a youth-like gradient profile exhibited a more youth-like profile also in D1DR distribution, and superior episodic memory.

Discussion

In this study, we present a comprehensive multidimensional characterization of functional hippocampal-neocortical integration across the adult human lifespan, and methodically map topography of connectivity gradients onto behavioral and molecular phenotypes. Our findings reveal the presence of two distinct connectivity gradients distributed along the hippocampus longitudinal axis which contribute to episodic memory function across the lifespan. These observations underscore the importance of disentangling multiple dimensions of hippocampal functional organization in advancing our understanding of cortico-hippocampal systems for memory-related behavior. Moreover, we demonstrate in two independent samples, that maintaining a youth-like gradient profile in older age – characterized by preserved distinctiveness of connectivity change along gradients – supports mnemonic functioning, and that increased homogeneity of gradient topography may precede gray matter atrophy.

Despite converging evidence in young adults indicating multiple overlapping modes of functional connectivity across the hippocampus[21,29–32], significant questions have remained regarding their spatial distribution across cortex, and their role in behavior. Here, connectopic mapping[57] identified a principal anteroposterior gradient (G1); a second-order gradient of mid-to-anterior/posterior long-axis variation (G2); and a third-order gradient conveying variation across the hippocampus transverse axis (G3). Although we restrict our discussion of G3 given its low proportion of explained variance, we note that it mirrors patterns previously observed in both structure and function[13,31,67]. Consistently, cortical patterns of G3 matched cortical connectivity profiles previously reported for hippocampal subfields[29,62]. Our results confirm that functional data favors detection of anteroposterior hippocampal organization in contrast to that determined by its cytoarchitecture[21], but indicate that higher-order connectivity modes may indeed carry coarse-scale information about subfield-determined organization. Greater anatomical specificity, with more precise characterization of connectivity

in relation to subfield boundaries while minimizing effects of inter-individual differences in hippocampal shape and folding, might be achieved by adopting techniques implementing a geodesic coordinate system to represent effects within the hippocampus[68,69].

The general organization of neocortical connectivity within the hippocampus showed stability across the lifespan (Figure 1), although clear effects of age were evident in the fine-scale topography of connectivity modes (Figure 4). Older age was associated with less distinct transitions in connectivity along G1 and G2, an effect that was exacerbated in a subgroup of older adults exhibiting an aged gradient profile – separated from older adults exhibiting youth-like gradient topography (Figure 6A-B). This finding constitutes an important addition to evidence highlighting increased homogeneity in hippocampal function in aging[44,70]. Current theories view this loss of specificity as a consequence of its functional isolation from neocortical areas, possibly linked to tau-driven degeneration of the perforant pathway[44,71]. Age-related deterioration of this entorhinal-hippocampal pathway has in turn been linked to impaired mnemonic functioning[72]. Importantly, older individuals exhibiting dedifferentiated gradient topography, but comparable hippocampal volumes, displayed less efficient episodic memory compared to older adults maintaining youth-like gradient topography (Figure 6; Supplementary Figure 7). This underscores the potential of gradient-based techniques to capture behaviorally relevant alterations in hippocampal function at a stage preceding structural decline.

Testing the correspondence across cortex of G1 and G2 to canonical gradients of cortical function provided support for G1 reflecting differentiation along a representation-modulation dimension (e.g., task-negative/task-positive[35]; Figure 1C-E), separating frontoparietal areas of attention and control from sensorimotor and DMN areas. Consistent with age-related loss of segregation between task-positive and task-negative poles[45], also evident in numerous diseases involving hippocampal dysfunction (e.g., depression[73], schizophrenia[74], and Alzheimer's disease[46]), we observed altered cortical organization of G1 in both older

subgroups. A main difference between subgroups, however, included a unimodal-transmodal organization instead emerging in youth-like older adults, whereas not in the aged subgroup (Figure 6D). A meaningful role of this potential reorganization was indicated by an association between G1 topography and memory in the youth-like older adults only. In terms of G2, we provide support of its characterization as a local representation of the principal unimodal-transmodal cortical gradient (Figure 1C-E), widely demonstrated across functional, structural, and molecular modalities[33,34,75]. Taken together, our observations support a framework of cortico-hippocampal integration in which the DMN is positioned in different neural contexts: in one case at the opposite end from frontoparietal networks of attention and control, and in the other, opposite to sensorimotor and visual networks – indicating that an account of the hippocampus functional connectivity with the DMN is dependent on multiple neurofunctional hierarchies. The overlap of G1 and G2 may potentially reflect the superimposition of gradients and hubs of long-axis anatomical connections indicated in both the human and animal hippocampus[20,76]. Moreover, the observation that macroscale relationships between distinct cortical systems are mapped out by G1 and G2 in this manner may reflect the hippocampus primordial position in the laminar development of the cerebral cortex[77], supporting the idea that hippocampal function stands, from a phylogenetic perspective, to inform general principles of brain organization[21].

We discovered that G2, specifically, manifested organizational principles shared among function, behavior, and neuromodulation. Meta-analytical decoding reproduced a unimodal-associative axis across G2 (Figure 3B), and analyses in relation to the distribution of D1DRs – which vary across cortex along a unimodal-transmodal axis[78,79] – demonstrated topographic correspondence both at the level of individual differences and across the group. It should, however, be acknowledged that PET imaging in the hippocampus is associated with resolution-related limitations, although previous research indicate high test-retest reliability of

[^{11}C]SCH23390 PET to quantify D1DR availability in this region[80]. As such, mapping the distribution of hippocampal D1DRs at a fine spatial scale remains challenging, and replication of our results in terms of overlap with G2 is needed in independent samples. Here, we evaluated the observed spatial overlap between G2 topography and D1DRs across multiple TSM model orders, showing correspondence between modalities from simple to more complex parameterizations of their spatial properties. Topographic correspondence was additionally observed between G2 and other DA markers from independent datasets (Figure 3B), suggesting that G2 may constitute a mode reflecting a dopaminergic phenotype, which contributes to the currently limited understanding of its biological underpinnings.

Results linked both G1 and G2 to episodic memory, suggesting complimentary contributions of these two overlapping long-axis modes. Considered together, analyses in the main and replication datasets indicated a role of G2 topography in memory across the adult lifespan, independent of age. A similar association with G1 was only evident across the entire sample in the replication dataset, whereas results in the main sample seemed to emphasize a role of youth-like G1 topography in memory performance. In line with previous research, memory was successfully predicted by G1 topography in young adults[30], and similarly predicted by G1 in older adults exhibiting a youth-like functional profile.

It is noteworthy that meta-analytical decoding of G2 primarily linked the unimodal connectivity patterns of anterior and posterior subregions to terms of episodic memory, encoding, and navigation (Figure 2C). G2's role in memory might as such be considered in light of hippocampal integration with the visual system, by which it contributes to complex perceptual processes supporting memory[81]. In humans, there is evidence of direct hippocampal connections to early visual areas, with recent tractography-based work demonstrating connectivity as primarily localized to the posterior hippocampus and to a smaller region in the anterior hippocampus[76].

The verbal nature of our memory tasks likely contributed to the left-lateralization of effects, yet, predominant left-hemisphere vulnerability to aging and age-related pathology should not be ruled out as a meaningful contributor to these effects[82]. Average hippocampal D1DR availability did not differ between older subgroups, but a tendency towards youth-like and aged functional profiles being mirrored in D1DR topography was observed (Figure 6E). However, longitudinal data is ultimately required to inform the underlying mechanisms of individual differences in hippocampal gradient topography in older age[83,84]. Future studies should, furthermore, assess gradients' modulation by behavioral conditions and extend these methods to clinical samples characterized by hippocampal dysfunction.

This study establishes behavioral relevance of two overlapping long-axis modes of hippocampal-neocortical functional connectivity, shedding light on their age-related dedifferentiation, and its impact on cognition. In sum, this study introduces a multidimensional framework for understanding hippocampal-neocortical integration and its interplay with memory and neuromodulation throughout the adult human lifespan.

Materials and Methods

This study included data from the DopamiNe, Age, connectoMe, and Cognition (DyNAMiC) study, for which the design and procedures have been described in detail elsewhere[58,85]. Here, we include the materials and methods relevant to the current study. DyNAMiC was approved by the Regional Ethical board and the local Radiation Safety Committee of Umeå, Sweden. All participants provided written informed consent prior to testing.

Participants

The DyNAMiC sample included 180 participants (20-79 years; mean age = 49.8±17.4; 90 men/90 women equally distributed within each decade). Individuals were randomly selected from the population register of Umeå, Sweden, and recruited via postal mail. Exclusion criteria implemented during the recruitment procedure included brain pathology, impaired cognitive functioning (Mini Mental State Examination < 26), medical conditions and treatment that could affect brain functioning and cognition (e.g. dementia, diabetes, and psychiatric diagnosis), and brain imaging contraindications (e.g. metal implants). All participants were native Swedish speakers. A total of 16 participants were excluded from connectopic mapping due to excessive in-scanner motion, leaving resting-state fMRI data for 164 participants (20-78 years; mean age = 48.7±17.3). As a replication data set, we used an independent sample of 224 cognitively healthy and native Swedish-speaking adults (122 men/102 women; 29-85 years mean age = 65.0±13.0) from the population-based Betula project, for which the design and recruitment procedures have been reported in detail elsewhere[59].

Episodic memory

Episodic memory was measured using three tasks testing word recall, number-word recall and object-location recall, respectively[58]. In the word recall task, participants were presented with

16 Swedish concrete nouns that appeared successively on a computer screen. Each word was presented for 6 s during encoding with an inter-stimulus interval (ISI) of 1 s. Following encoding, participants reported as many words as they could recall by typing them using the keyboard. Two trials were completed, yielding a maximum score of 32. In the number-word task, participants encoded pairs of 2-digit numbers and concrete plural nouns (e.g., 46 dogs). During encoding, eight number-word pairs were presented, each displayed for 6 s, with an ISI of 1 s. Following encoding, nouns were presented again, in a re-arranged order, and participants had to report the 2-digit number associated with each presented noun (e.g. How many dogs?). This task included two trials with a total maximum score of 16. The third task was an object-location memory task. Here, participants were presented with a 6 × 6 square grid in which 12 objects were, one by one, shown at distinct locations. Each object-position pairing was displayed for 8 s, with an ISI of 1 s. Following encoding, all objects were simultaneously shown next to the grid for the participant to move them (in any order) to their correct position in the grid. If unable to recall the correct position of an object, participants had to guess and place the object in the grid to the best of their ability. Two trials of this task were completed, making the total maximum score 24.

A composite score of performances across the three tasks was calculated and used as the measure of episodic memory. For each of the three tasks, scores were summarized across the total number of trials. The three resulting sum scores were z-standardized and averaged to form one composite score of episodic memory performance (T score: mean = 50; SD = 10). Missing values were replaced by the average of the available observed scores.

Image acquisition

Brain imaging was conducted at Umeå University Hospital, Sweden. Structural and functional MRI data were acquired with a 3T Discovery MR 750 scanner (General Electric, WI, USA),

using a 32-channel head coil. Positron emission tomography (PET) data were acquired with a Discovery PET/CT 690 scanner (General Electric, WI, USA).

Structural MR Imaging

Anatomical T1-weighted images were acquired with a 3D fast-spoiled gradient-echo sequence, collected as 176 slices with a thickness of 1 mm. Repetition time (TR) was 8.2 ms, echo-time (TE) = 3.2 ms, flip angle = 12º, and field of view (FOV) = 250 × 250 mm.

Functional MR Imaging

Functional MR data were collected during resting-state, with participants instructed to keep their eyes open and focus on a fixation cross during scanning. Images were acquired using a T2*-weighted single-shot echo-planar imaging (EPI) sequence, with a total of 350 volumes collected over 12 minutes. The functional time series was sampled with 37 transaxial slices, slice thickness = 3.4 mm, and 0.5 mm spacing, TR = 2000 ms, TE = 30 ms, flip angle = 80º, and FOV = 250 x 250 mm. Ten dummy scans were collected at the start of the sequence.

PET Imaging

PET was conducted in 3D mode with a Discovery PET/CT 690 (General Electric, WI, US) to assess whole-brain dopamine D1 receptor availability using the radioligand [^{11}C]SCH23390. Scanning was done during a resting condition, with participants instructed to lay still and remain awake with their eyes open. To minimize head movement, a thermoplastic mask (Posicast®; CIVCO medical solutions; IA, US) was individually fitted for each participant, and attached to the bed surface during scanning. Following a low-dose CT scan (10 mA, 120 kV, and 0.8 s rotation time) for attenuation correction, an intravenous bolus injection with target radioactivity of 350 MBq [^{11}C]SCH23390 was administered. The PET scan was a 60 min dynamic scan, with 6 x 10 s, 6 x 20 s, 6 x 40 s, 9 x 60 s, 22 x 120 s frames. The average radioactivity dose

administered to participants was 337±27 MBq (range 205-391 MBq). Due to participant drop-out and technical issues, complete PET data was available for 177 DyNAMiC participants.

Image preprocessing

Hippocampal segmentation and volumetric assessment

Individual anatomical T1-weighted images were submitted to automated segmentation in FreeSurfer version 6[86]. A mean image of participants' normalized T1-weighted images was also segmented in FreeSurfer, and yielded hippocampal and cortical segmentations used as masks for connectopic mapping. Regional gray matter (GM) volume was estimated from subject-specific hippocampal segmentations, and were corrected for total intracranial volume (ICV; the sum of volumes for grey matter, white matter, and cerebrospinal fluid). Adjusted volumes were equal to the raw volume - *b*(ICV - mean ICV), where *b* is the regression slope of volume on ICV[87]. Automated segmentation of the hippocampus into subiculum, CA1-3, and DG/CA4 subfields was conducted in FreeSurfer using the group-average T1-weighted image, for sample-specific masks to overlay onto G3 (Supplementary Figure 2).

Functional MRI data

Resting-state fMRI data were preprocessed using Statistical Parametric Mapping (SPM12: Wellcome Trust Centre for Neuroimaging, http://www.fil.ion.ucl.ac.uk/spm/) implemented in an in-house software, DataZ. Functional images were slice-timing corrected, co-registered to the anatomical T1-images, and motion corrected, and underwent distortion correction using subject-specific B0-field maps. The functional data were subsequently co-registered to the anatomical T1-images again, temporally demeaned and linear and quadratic effects were removed. Next, a 36-parameter nuisance regression model was applied[88], including mean cerebrospinal, white-matter, and whole-brain signal in addition to six motion parameters, including parameters' squares, derivatives, and squared derivatives. To further control for in-

scanner motion, the model also included a set of spike regressors, defined as binary vectors of motion-contaminated volumes exceeding a volume-to-volume root-mean-squared (RMS) displacement of 0.25 mm. A temporal high-pass filter (with a threshold of 0.009 Hz) was applied simultaneously as nuisance regression in order to not re-introduce nuisance signals. Finally, images were normalized to MNI space by Diffeomorphic Anatomical Registration using Exponentiated Lie algebra (DARTEL[89]) and smoothed with a 6-mm FWHM Gaussian kernel. Four individuals were excluded from the template-generation step due to non-pathological anatomical irregularities. In total, 16 participants were excluded due to displaying excessive in-scanner motion, as defined by displaying i) more than 20 volumes with >0.25 relative RMS difference in motion, and ii) greater than 0.2 average RMS across the run. On average, the relative RMS difference in motion across the sample was 0.090 (± 0.063), and the mean frame-wise displacement (FD) was 0.164 (± 0.104).

Dopamine D1 receptor availability

Preprocessing of PET data was performed in SPM12 (Wellcome Trust Centre for Neuroimaging, http://www.fil.ion.ucl.ac.uk/spm/). Binding potential relative to non-displaceable binding in a reference region (BP_{ND}; Innis et al., 2007), was used as an estimate of receptor availability (i.e. D1DR) in the hippocampus, for each participant defined using the FreeSurfer segmentation of their anatomical images. Cerebellum was used as reference region. PET images were corrected for head movement by using frame-to-frame image co-registration, and co-registered with T1-weighted MRI images with re-slicing to T1 voxel size. The simplified reference-tissue model (SRTM) was used to model regional time-activity course (TAC) data. Regional TAC data were adjusted for partial volume effects (PVE) by using the symmetric geometric transfer matrix (SGTM) method implemented in FreeSurfer, and an estimated point-spread-function of 2.5 mm full-width-at-half-maximum (FWHM). We additionally used data from a publicly available database of group-averaged volumetric maps of molecular target

distributions (https://github.com/netneurolab/hansen_receptors). Specifically, we downloaded previously published maps of DAT[65] and FDOPA (https://www.nitrc.org/projects/spmtemplates), to investigate the spatial correspondence between functional gradients and dopaminergic target distributions.

Mapping gradients of functional connectivity

Connectopic mapping[57] was run through the ConGrads toolbox[57] implemented in FSL[91]. Mapping was conducted on both subject level and group level, for the left and right hippocampus separately, and involved two main steps. First, for every hippocampal voxel, connectivity fingerprints were computed as the Pearson correlation between the voxel-wise time-series and a singular-value decomposition (SVD) representation of all cortical voxels. In a second step, non-linear manifold learning (Laplacian eigenmaps) was applied to a matrix expressing the degree of similarity between the voxel-wise fingerprints. This yields eigenvectors, so called connectopic maps, representing modes of functional connectivity (i.e. functional gradients). Each connectopic map is then projected onto cortex, for which each vertex is color coded according to the voxel in the hippocampus it correlates the most with. Since connectopic mapping at group level involves applying Laplacian eigenmaps to a group-average similarity matrix, group level mapping across the sample was conducted using the hippocampal and cortical masks derived from the FreeSurfer segmentation of a sample-mean structural image. Mapping was specified to compute 20 gradients, and a subsequent scree plot over explained variance indicated meaningful contributions of the three first connectopic maps, together explaining 67% of the variance across hemispheres (Supplementary Figure 1).

Stability of functional gradients across levels of spatial smoothing

It has recently been suggested that the reliability of connectopic mapping to detect meaningful gradients of resting-state functional connectivity may be limited due to spatial smoothing

implemented during preprocessing of fMRI data[60]. To determine the stability of our hippocampal gradients, we conducted a series of control analyses across varying levels of smoothing, and in contrast to connectopic maps derived through connectopic mapping on random data. These analyses are presented in the Supplementary Information, and confirmed high stability of resting-state gradients and their ability to capture inter-individual differences, whereas random data failed to produce meaningful gradients (Supplementary Figure 4).

Alignment of connectopic maps across participants

To ensure optimal alignment of identified connectopic maps across participants, we employed Procrustes alignment, based on voxel-wise correlations, to order subject-level connectopic maps according to their correspondence with a set of reference maps (i.e. gradients computed at group level across the full sample). Moreover, whereas the sign of connectopic maps is arbitrary, differences therein have an impact on the spatial model parameters describing the topographic characteristics of gradients, derived through TSM in a later step. As such, the sign of subject-level connectopic maps showing negative correlations with the corresponding group-level reference map were inversed.

Trend surface modelling

Using spatial statistics, the topography of a connectopic map can be represented by a small number of spatial model parameters. This parameterization enables analyses of inter-individual differences, and is achieved through trend surface modelling (TSM), implemented in a third step of the ConGrads analysis pipeline[57]. In this step, the spatial pattern of each subject-level connectopic map is approximated by estimating a spatial statistical model. Model estimation involves fitting a set of polynomial basis functions along canonical axes of the connectopic map. In MNI space, this entails estimation along x, y, and z axes of the hippocampus. Thus, fitting a polynomial of degree 1 yields three TSM parameters (x, y, z), with any increase in model order corresponding to an increase in number of parameters (e.g. 6 parameters for the

second model order: x, y, z, x^2, y^2, z^2; 9 parameters for the third model order, etc.). Trend surface models are fitted with an increasing polynomial degree using Bayesian linear regression, which provides likelihood estimates that can be used for subsequent model selection. Here, model selection was based on three information sources: a) the Bayesian Information Criterion (BIC) across subjects for models estimated at orders 1-10; b) the % explained variance in connectopic maps by each model; and c) visual inspection of group-level gradients reconstructed from TSM parameters at different model orders. The purpose of using multiple information sources, as opposed to simply BIC, was to find a trade-off between high-quality reconstructions of gradients by TSM models, while keeping the number of model parameters sufficiently low for multivariate statistical analyses. A model order of 3 (=9 TSM parameters) was selected for G1, whereas a model order of 4 (=12 TSM parameters) was selected for G2 and G3 (Supplementary Figure 5). Each gradient's set of TSM parameters were then used as either dependent or independent variables in multivariate GLMs investigating links between gradient topography and variables such as age, episodic memory performance, and D1DR distribution.

Transitions in connectivity as a function of the hippocampal longitudinal axis

To visualize the orthogonal patterns of change in connectivity conveyed by each gradient, and to aid in the interpretation of age effects, we divided each subject-level connectopic map into 23 bins of ~2mm along the hippocampus anterior-posterior axis and estimated the average gradient value (ranging from 0-1) for each bin. Plotting the values of each bin against their distance in mm from the most anterior voxel in the hippocampus as such demonstrates the pattern of change in connectivity along the anterior-posterior axis[30].

Cortical projections and correlations with gradients of cortical function

In ConGrads[57], cortical mapping is computed independently for each gradient based on the regression equation: $pmap = \boldsymbol{B^T}.(\boldsymbol{X^{T^{-1}}}.\boldsymbol{A^T})^T$ where A corresponds to data inside (i.e.,

hippocampus) and B to data outside (i.e., cortical) the ROI, and X-1 is the pseudo-inverse of the corresponding eigenvector (stacked with a row of ones). For each hippocampal gradient, the volumetric MNI-registered group-level cortical projection map was resampled to the Human Connectome Project 32k_LR midthickness surface mesh, using the volume-to-surface algorithm with enclosing mapping available in Connectome Workbench v.1.5.0. Spearman correlations were computed between the cortical projection of each hippocampal gradient and the three gradients previously established as the main axes of cortical functional organization[34]. To reduce the degree of freedom, each surface projection was resampled by 1000-cortical parcels[92]. Statistical significance of correlations was assessed by spin-test permutation[93], randomly rotating a spherical projection of the cortical maps 1000 times, with two-tailed statistical significance determined at a 95% confidence level.

Mapping behavioral transitions along gradients using Neurosynth

Transitions in behavioral domains were mapped onto G1 and G2 using meta-analytical decoding in Neurosynth[63]. We assessed two sets of behavioral terms (Figure 2), the first was a selection of terms commonly linked to anteroposterior hippocampal functional specialization[13,14], and the second a selection of terms based on a previous report demonstrating behavioral transitions along a unimodal-transmodal cortical axis[34]. For correspondence with meta-analytical maps, we created region of interest masks by projecting the cortical surface of each gradient to the 2-mm volumetric MNI152 standard space. These volumetric images were then divided into five twenty-percentile bins and binarized. The resulting images were used as input to the Neurosynth decoder, yielding an *r* statistic associated with each behavioral term per section of each gradient.

Acknowledgements

This work was supported by the Swedish Research Council (grant number 2016-01936 to A.S.), Riksbankens Jubileumsfond (grant number P20-0515 to A.S.), Knut and Alice Wallenberg Foundation (Wallenberg Fellow grant to A.S.), and StratNeuro grant at Karolinska Institutet (A.S.). The Betula Study is supported by a Scholar grant to L.N. from the Knut and Alice Wallenberg Foundation. FreeSurfer calculations were enabled by resources provided by the Swedish National Infrastructure for Computing (SNIC) at HPC2N, partially funded by the Swedish Research Council through grant agreement no. 2018-05973.

Author contributions

K.N., A.S., A.R, and F.G. conceived the study idea. F.F., M.A., J.J., R.P., A.A., and K.N. performed the data processing and formal analysis. All authors contributed to the interpretation of the findings. K.N. and A.S. wrote the manuscript with valuable feedback and revision by R.P., F.F., J.J., F.G., M.A., S.K., L.B., A.Z., A.R., and L.N.

Data and code availability

Data from the DyNAMiC study are not publicly available. Access to the original data may be shared upon request from the Principal investigator, Dr. Alireza Salami. The Matlab, R, and FSL codes used for analyses included in this study are openly available at https://github.com/kristinnordin/hcgradients. Computation of gradients was done using the freely available toolbox ConGrads: https://github.com/koenhaak/congrads.

Ethical approval

This study was approved by the Regional Ethical board and the local Radiation Safety Committee in Umeå, Sweden.

Declaration of interests

The authors declare no competing interests.

References

1. Laurita, A. C. & Spreng, N. The Hippocampus and Social Cognition. in *The Hippocampus from Cells to Systems: Structure, Connectivity, and Functional Contributions to Memory and Flexible Cognition* (eds. Hannula, D. E. & Duff, M. C.) 537–558 (Springer International Publishing, Cham, 2017). doi:10.1007/978-3-319-50406-3_17.
2. Moscovitch, M., Cabeza, R., Winocur, G. & Nadel, L. Episodic memory and beyond: the hippocampus and neocortex in transformation. *Annu. Rev. Psychol.* **67**, 105–134 (2016).
3. Nadel, L. & Peterson, M. A. The hippocampus: Part of an interactive posterior representational system spanning perceptual and memorial systems. *J. Exp. Psychol. Gen.* **142**, 1242–1254 (2013).
4. Ranganath, C. & Ritchey, M. Two cortical systems for memory-guided behaviour. *Nat. Rev. Neurosci.* **13**, 713–726 (2012).
5. Barnes, J. *et al.* A meta-analysis of hippocampal atrophy rates in Alzheimer's disease. *Neurobiol. Aging* **30**, 1711–1723 (2009).
6. Campbell, S. & MacQueen, G. The role of the hippocampus in the pathophysiology of major depression. *J. Psychiatry Neurosci.* **29**, 417–426 (2004).
7. Harrison, P. J. The hippocampus in schizophrenia: a review of the neuropathological evidence and its pathophysiological implications. *Psychopharmacology (Berl.)* **174**, 151–162 (2004).
8. Xie, L. *et al.* Longitudinal atrophy in early Braak regions in preclinical Alzheimer's disease. *Hum. Brain Mapp.* **41**, 4704–4717 (2020).
9. Amaral, D. G. & Witter, M. P. The three-dimensional organization of the hippocampal formation: A review of anatomical data. *Neuroscience* **31**, 571–591 (1989).
10. Witter, M. P. & Amaral, D. G. The entorhinal cortex of the monkey: VI. Organization of projections from the hippocampus, subiculum, presubiculum, and parasubiculum. *J. Comp. Neurol.* **529**, 828–852 (2021).
11. Amunts, K. *et al.* Cytoarchitectonic mapping of the human amygdala, hippocampal region and entorhinal cortex: intersubject variability and probability maps. *Anat. Embryol. (Berl.)* **210**, 343–352 (2005).
12. Libby, L. A., Ekstrom, A. D., Ragland, J. D. & Ranganath, C. Differential connectivity of perirhinal and parahippocampal cortices within human hippocampal subregions revealed by high-resolution functional imaging. *J. Neurosci.* **32**, 6550–6560 (2012).
13. Plachti, A. *et al.* Multimodal parcellations and extensive behavioral profiling tackling the hippocampus gradient. *Cereb. Cortex* **29**, 1–18 (2019).
14. Grady, C. Meta-analytic and functional connectivity evidence from functional magnetic resonance imaging for an anterior to posterior gradient of function along the hippocampal axis. *Hippocampus* **2019**, 1–16 (2019).
15. Poppenk, J., Evensmoen, H. R., Moscovitch, M. & Nadel, L. Long-axis specialization of the human hippocampus. *Trends Cogn. Sci.* **17**, 230–240 (2013).
16. Lladó, A. *et al.* The hippocampal longitudinal axis—relevance for underlying tau and TDP-43 pathology. *Neurobiol. Aging* **70**, 1–9 (2018).

17. Small, S. A., Schobel, S. A., Buxton, R. B., Witter, M. P. & Barnes, C. A. A pathophysiological framework of hippocampal dysfunction in ageing and disease. *Nat. Rev. Neurosci.* **12**, 585–601 (2011).
18. Dalton, M. A., McCormick, C. & Maguire, E. A. Differences in functional connectivity along the anterior-posterior axis of human hippocampal subfields. *NeuroImage* **192**, 38–51 (2019).
19. Aggleton, J. P. Multiple anatomical systems embedded within the primate medial temporal lobe: Implications for hippocampal function. *Neurosci. Biobehav. Rev.* **36**, 1579–1596 (2012).
20. Strange, B. A., Witter, M. P., Lein, E. S. & Moser, E. I. Functional organization of the hippocampal longitudinal axis. *Nat. Rev. Neurosci.* **15**, 655–669 (2014).
21. Genon, S., Bernhardt, B. C., La Joie, R., Amunts, K. & Eickhoff, S. B. The many dimensions of human hippocampal organization and (dys)function. *Trends Neurosci.* (2021) doi:10.1016/j.tins.2021.10.003.
22. Spreng, R. N., Mar, R. A. & Kim, A. S. N. The Common Neural Basis of Autobiographical Memory, Prospection, Navigation, Theory of Mind, and the Default Mode: A Quantitative Meta-analysis. *J. Cogn. Neurosci.* **21**, 489–510 (2008).
23. Adnan, A. *et al.* Distinct hippocampal functional networks revealed by tractography-based parcellation. *Brain Struct. Funct.* **221**, 2999–3012 (2016).
24. Poppenk, J. & Moscovitch, M. A hippocampal marker of recollection memory ability among healthy young adults: contributions of posterior and anterior segments. *Neuron* **72**, 931–937 (2011).
25. Blessing, E. M., Beissner, F., Schumann, A., Brünner, F. & Bär, K.-J. A data-driven approach to mapping cortical and subcortical intrinsic functional connectivity along the longitudinal hippocampal axis. *Hum. Brain Mapp.* **37**, 462–476 (2016).
26. Chase, H. W. *et al.* Evidence for an anterior–posterior differentiation in the human hippocampal formation revealed by meta-analytic parcellation of fMRI coordinate maps: Focus on the subiculum. *NeuroImage* **113**, 44–60 (2015).
27. Zhong, Q. *et al.* Functional parcellation of the hippocampus from resting-state dynamic functional connectivity. *Brain Res.* **1715**, 165–175 (2019).
28. Langnes, E. *et al.* Anterior and posterior hippocampus macro- and microstructure across the lifespan in relation to memory—A longitudinal study. *Hippocampus* 1–15 (2020) doi:10.1002/hipo.23189.
29. vos de Wael, R. *et al.* Anatomical and microstructural determinants of hippocampal subfield functional connectome embedding. *Proc. Natl. Acad. Sci.* **115**, 10154–10159 (2018).
30. Przeździk, I., Faber, M., Fernández, G., Beckmann, C. F. & Haak, K. V. The functional organisation of the hippocampus along its long axis is gradual and predicts recollection. *Cortex* **119**, 324–335 (2019).
31. Katsumi, Y. *et al.* Correspondence of functional connectivity gradients across human isocortex, cerebellum, and hippocampus. *Commun. Biol.* **6**, 1–13 (2023).
32. Tian, Y., Margulies, D. S., Breakspear, M. & Zalesky, A. Topographic organization of the human subcortex unveiled with functional connectivity gradients. *Nat. Neurosci.* **23**, 1421–1432 (2020).

33. Huntenburg, J. M., Bazin, P.-L. & Margulies, D. S. Large-Scale Gradients in Human Cortical Organization. *Trends Cogn. Sci.* **22**, 21–31 (2018).
34. Margulies, D. S. *et al.* Situating the default-mode network along a principal gradient of macroscale cortical organization. *Proc. Natl. Acad. Sci.* **113**, 12574–12579 (2016).
35. Fox, M. D. *et al.* The human brain is intrinsically organized into dynamic, anticorrelated functional networks. *Proc. Natl. Acad. Sci.* **102**, 9673–9678 (2005).
36. Ge, R. *et al.* Parcellation of the human hippocampus based on gray matter volume covariance: Replicable results on healthy young adults. *Hum. Brain Mapp.* **0**, (2019).
37. Vogel, J. W. *et al.* A molecular gradient along the longitudinal axis of the human hippocampus informs large-scale behavioral systems. *Nat. Commun.* **11**, 960 (2020).
38. Van Essen, D. C. *et al.* The WU-Minn Human Connectome Project: An overview. *NeuroImage* **80**, 62–79 (2013).
39. Damoiseaux, J. S., Viviano, R. P., Yuan, P. & Raz, N. Differential effect of age on posterior and anterior hippocampal functional connectivity. *NeuroImage* **133**, 468–476 (2016).
40. Salami, A., Wåhlin, A., Kaboodvand, N., Lundquist, A. & Nyberg, L. Longitudinal evidence for dissociation of anterior and posterior MTL resting-state connectivity in aging: links to perfusion and memory. *Cereb. Cortex* **26**, 3953–3963 (2016).
41. Nyberg, L., Andersson, M., Lundquist, A., Salami, A. & Wåhlin, A. Frontal contribution to hippocampal hyperactivity during memory encoding in aging. *Front. Mol. Neurosci.* **12**, 1–11 (2019).
42. Salami, A., Pudas, S. & Nyberg, L. Elevated hippocampal resting-state connectivity underlies deficient neurocognitive function in aging. *Proc. Natl. Acad. Sci.* **111**, 17654–17659 (2014).
43. Berron, D. *et al.* Early stages of tau pathology and its associations with functional connectivity, atrophy and memory. *Brain* **144**, 2771–2783 (2021).
44. Harrison, T. M. *et al.* Tau deposition is associated with functional isolation of the hippocampus in aging. *Nat. Commun.* **10**, 1–12 (2019).
45. Grady, C., Sarraf, S., Saverino, C. & Campbell, K. Age differences in the functional interactions among the default, frontoparietal control, and dorsal attention networks. *Neurobiol. Aging* **41**, 159–172 (2016).
46. Weiler, M. *et al.* Intranetwork and internetwork connectivity in patients with Alzheimer disease and the association with cerebrospinal fluid biomarker levels. *J. Psychiatry Neurosci.* **42**, 366–377 (2017).
47. Edelmann, E. & Lessmann, V. Dopaminergic innervation and modulation of hippocampal networks. *Cell Tissue Res.* **373**, 711–727 (2018).
48. El-Ghundi, M., O'Dowd, B. F. & George, S. R. Insights into the role of dopamine receptor systems in learning and memory. *Rev. Neurosci.* **18**, 37–66 (2007).
49. Seamans, J. K. & Yang, C. R. The principal features and mechanisms of dopamine modulation in the prefrontal cortex. *Prog. Neurobiol.* **74**, 1–58 (2004).
50. Pedersen, R., Johansson, J. & Salami, A. Dopamine D1-signaling modulates maintenance of functional network segregation in aging. *Aging Brain* **3**, 100079 (2023).

51. Gasbarri, A., Verney, C., Innocenzi, R., Campana, E. & Pacitti, C. Mesolimbic dopaminergic neurons innervating the hippocampal formation in the rat: a combined retrograde tracing and immunohistochemical study. *Brain Res.* **668**, 71–79 (1994).
52. Kempadoo, K. A., Mosharov, E. V., Choi, S. J., Sulzer, D. & Kandel, E. R. Dopamine release from the locus coeruleus to the dorsal hippocampus promotes spatial learning and memory. *Proc. Natl. Acad. Sci.* **113**, 14835–14840 (2016).
53. Dubovyk, V. & Manahan-Vaughan, D. Gradient of expression of dopamine D2 receptors along the dorso-ventral axis of the hippocampus. *Front. Synaptic Neurosci.* **11**, (2019).
54. Kahn, I. & Shohamy, D. Intrinsic connectivity between the hippocampus, nucleus accumbens and ventral tegmental area in humans. *Hippocampus* **23**, 187–192 (2013).
55. Nordin, K. *et al.* Distinct and Common Large-Scale Networks of the Hippocampal Long Axis in Older Age: Links to Episodic Memory and Dopamine D2 Receptor Availability. *Cereb. Cortex* **31**, 3435–3450 (2021).
56. Pedersen, R. *et al.* Dopamine D1-receptor Organization Contributes to Functional Brain Architecture. *J. Neurosci.* (2024) doi:10.1523/JNEUROSCI.0621-23.2024.
57. Haak, K. V., Marquand, A. F. & Beckmann, C. F. Connectopic mapping with resting-state fMRI. *NeuroImage* **170**, 83–94 (2018).
58. Nordin, K. *et al.* DyNAMiC: A prospective longitudinal study of dopamine and brain connectomes: A new window into cognitive aging. *J. Neurosci. Res.* 1–25 (2022) doi:10.1002/jnr.25039.
59. Nilsson, L.-G. *et al.* Betula: A Prospective Cohort Study on Memory, Health and Aging. *Aging Neuropsychol. Cogn.* **11**, 134–148 (2004).
60. Watson, D. M. & Andrews, T. J. Connectopic mapping techniques do not reflect functional gradients in the brain. *NeuroImage* 120228 (2023) doi:10.1016/j.neuroimage.2023.120228.
61. Yeo, B. T. *et al.* The organization of the human cerebral cortex estimated by intrinsic functional connectivity. *J. Neurophysiol.* **106**, 1125–1165 (2011).
62. de Flores, R. *et al.* Intrinsic connectivity of hippocampal subfields in normal elderly and mild cognitive impairment patients. *Hum. Brain Mapp.* **38**, 4922–4932 (2017).
63. Yarkoni, T., Poldrack, R. A., Nichols, T. E., Van Essen, D. C. & Wager, T. D. Large-scale automated synthesis of human functional neuroimaging data. *Nat. Methods* **8**, 665–670 (2011).
64. Haak, K. V. & Beckmann, C. F. Understanding brain organisation in the face of functional heterogeneity and functional multiplicity. *NeuroImage* **220**, 117061 (2020).
65. Dukart, J. *et al.* Cerebral blood flow predicts differential neurotransmitter activity. *Sci. Rep.* **8**, 4074 (2018).
66. Oldehinkel, M. *et al.* Mapping dopaminergic projections in the human brain with resting-state fMRI. *eLife* **11**, e71846 (2022).
67. Thorp, J. N., Gasser, C., Blessing, E. & Davachi, L. Data-Driven Clustering of Functional Signals Reveals Gradients in Processing Both within the Anterior Hippocampus and across Its Long Axis. *J. Neurosci.* **42**, 7431–7441 (2022).
68. DeKraker, J. *et al.* Automated hippocampal unfolding for morphometry and subfield segmentation with HippUnfold. *eLife* **11**, e77945 (2022).

69. Paquola, C. *et al.* Convergence of cortical types and functional motifs in the human mesiotemporal lobe. *eLife* **9**, e60673 (2020).
70. Stark, S. M., Frithsen, A. & Stark, C. E. L. Age-related alterations in functional connectivity along the longitudinal axis of the hippocampus and its subfields. *Hippocampus* **31**, 11–27 (2021).
71. Hyman, B. T., Van Hoesen, G. W., Damasio, A. R. & Barnes, C. L. Alzheimer's Disease: Cell-Specific Pathology Isolates the Hippocampal Formation. *Science* **225**, 1168–1170 (1984).
72. Yassa, M. A., Muftuler, L. T. & Stark, C. E. L. Ultrahigh-resolution microstructural diffusion tensor imaging reveals perforant path degradation in aged humans in vivo. *Proc. Natl. Acad. Sci.* **107**, 12687–12691 (2010).
73. Mulders, P. C., van Eijndhoven, P. F., Schene, A. H., Beckmann, C. F. & Tendolkar, I. Resting-state functional connectivity in major depressive disorder: A review. *Neurosci. Biobehav. Rev.* **56**, 330–344 (2015).
74. Whitfield-Gabrieli, S. *et al.* Hyperactivity and hyperconnectivity of the default network in schizophrenia and in first-degree relatives of persons with schizophrenia. *Proc. Natl. Acad. Sci.* **106**, 1279–1284 (2009).
75. Hansen, J. Y. *et al.* Mapping gene transcription and neurocognition across human neocortex. *Nat. Hum. Behav.* **5**, 1240–1250 (2021).
76. Dalton, M. A., D'Souza, A., Lv, J. & Calamante, F. New insights into anatomical connectivity along the anterior–posterior axis of the human hippocampus using in vivo quantitative fibre tracking. *eLife* **11**, e76143 (2022).
77. Goulas, A., Margulies, D. S., Bezgin, G. & Hilgetag, C. C. The architecture of mammalian cortical connectomes in light of the theory of the dual origin of the cerebral cortex. *Cortex* **118**, 244–261 (2019).
78. Froudist-Walsh, S. *et al.* A dopamine gradient controls access to distributed working memory in the large-scale monkey cortex. *Neuron* **109**, 3500-3520.e13 (2021).
79. Pedersen, R. *et al.* Dopamine D1-receptor Organization Contributes to Functional Brain Architecture. Preprint at (2023).
80. Kaller, S. *et al.* Test–retest measurements of dopamine D1-type receptors using simultaneous PET/MRI imaging. *Eur. J. Nucl. Med. Mol. Imaging* **44**, 1025–1032 (2017).
81. Turk-Browne, N. B. The hippocampus as a visual area organized by space and time: A spatiotemporal similarity hypothesis. *Vision Res.* **165**, 123–130 (2019).
82. Minkova, L. *et al.* Gray matter asymmetries in aging and neurodegeneration: A review and meta-analysis. *Hum. Brain Mapp.* **38**, 5890–5904 (2017).
83. Nyberg, L., Lövdén, M., Riklund, K., Lindenberger, U. & Bäckman, L. Memory aging and brain maintenance. *Trends Cogn. Sci.* **16**, 292–305 (2012).
84. Cabeza, R. *et al.* Maintenance, reserve and compensation: the cognitive neuroscience of healthy ageing. *Nat. Rev. Neurosci.* **19**, 701–710 (2018).
85. Johansson, J. *et al.* Biphasic patterns of age-related differences in dopamine D1 receptors across the adult lifespan. *Cell Rep.* **42**, (2023).
86. Fischl, B. *et al.* Whole brain segmentation: Automated labeling of neuroanatomical structures in the human brain. *Neuron* **33**, 341–355 (2002).

87. Buckner, R. L. *et al.* A unified approach for morphometric and functional data analysis in young, old, and demented adults using automated atlas-based head size normalization: reliability and validation against manual measurement of total intracranial volume. *NeuroImage* **23**, 724–738 (2004).
88. Ciric, R. *et al.* Benchmarking of participant-level confound regression strategies for the control of motion artifact in studies of functional connectivity. *NeuroImage* **154**, 174–187 (2017).
89. Ashburner, J. A fast diffeomorphic image registration algorithm. *NeuroImage* **38**, 95–113 (2007).
90. Innis, R. B. *et al.* Consensus Nomenclature for in vivo Imaging of Reversibly Binding Radioligands: *J. Cereb. Blood Flow Metab.* **27**, 1533–1539 (2007).
91. Smith, S. M. *et al.* Advances in functional and structural MR image analysis and implementation as FSL. *NeuroImage* **23**, S208–S219 (2004).
92. Schaefer, A. *et al.* Local-Global Parcellation of the Human Cerebral Cortex from Intrinsic Functional Connectivity MRI. *Cereb. Cortex* **28**, 3095–3114 (2018).
93. Alexander-Bloch, A. F. *et al.* On testing for spatial correspondence between maps of human brain structure and function. *NeuroImage* **178**, 540–551 (2018).